Rock and Soil Mechanics

Volume 41 | Issue 1 Article 2

9-18-2020

Experimental study on dynamic shear modulus and damping ratio of coral sand from Nansha Islands

Ke LIANG

Yang HE

Guo-xing CHEN
gxc6307@163.com

Custom Citation

LIANG Ke, HE Yang, CHEN Guo-xing. Experimental study on dynamic shear modulus and damping ratio of coral sand from Nansha Islands [J]. Rock and Soil Mechanics, 2020, 41(1): 23-31.

Rock and Soil Mechanics 2020 41(1): 23−31 ISSN 1000−7598
https: //doi.org/10.16285/j.rsm.2018.7359 rocksoilmech.researchcommons.org/journal

Experimental study on dynamic shear modulus and damping ratio of coral sand from Nansha Islands

LIANG Ke[1], HE Yang[1], CHEN Guo-xing[1, 2]

1. Institute of Geotechnical Engineering, Nanjing Tech. University, Nanjing, Jiangsu, 210009, China

2. Civil Engineering and Earthquake Disaster Prevention Center of Jiangsu Province, Nanjing Tech. University, Nanjing, Jiangsu 210009, China

Abstract: The physical and engineering mechanical behaviors between coral sand and terrigenous sandy soils are considerably different. To study these behaviours, a series of undrained multistage strain-controlled cyclic triaxial tests were conducted on saturated coral sand from Nansha Islands, South China Sea. The influence of effective confining pressure p_0' and relative density D_r on the dynamic shear modulus and damping ratio of coral sand was studied. Compared with the test results of coral sand and terrigenous sandy soil and gravel, significant differences were found in the maximum shear modulus G_{max}, the shapes and the upper and lower boundaries of shear modulus ratio G/G_{max} curves, reference shear strains γ_0, the shapes and the upper and lower boundaries of damping ratio λ curves. The maximum shear modulus G_{max} of coral sand is higher than that of terrigenous sandy soil and gravel, and the G_{max} of coral sand predicted by empirical equations of terrigenous sandy soil is underestimated by 30%. The nonlinearity of coral sand is slightly weaker than that of terrigenous sandy soil and gravel. The empirical formulas for predicting G/G_{max} and λ of terrigenous sandy soil and gravel are not applicable for Nansha coral sand. The empirical formulas for predicting G/G_{max} and λ of coral sand are proposed.

Keywords: Nansha coral sand; the maximum shear modulus; shear modulus ratio; damping ratio; cyclic triaxial test

1 Introduction

Under the Belt and Road Initiative, the construction of coral reefs in South China Sea is proceeding. Coral sand is the main geotechnical material in coral reefs, with the major component of calcium minerals, which is the product of coral body due to geologic processes, such as transportation and deposition. The particles of coral sand have many characteristics, including many pores (with inner pore), irregular shape, high angularity, high fragility and easily cemented, etc. Therefore, the engineering properties of coral sand are significantly different from common terrigenous and marine sediments. The seismic ground failure of coral sand site occurred several times, such as the 1993 Guam Mw 7.7 Earthquake[1] and the 2006 Hawaii Mw 6.7 Earthquake[2], both of which induced ground liquefication and lateral spreading in large areas of coral sand sites, causing severe damages to port infrastructure and other shoreline structures. Therefore, the dynamic properties of saturated coral sand attracted more attentions from researchers.

The liquefaction properties of saturated coral sand have been investigated by many researchers[3-5]. Currently, many researchers have reached consensus that the liquefaction resistance of saturated coral sand is higher than common quartz sand. Some studies have been conducted on the dynamic shear modulus and damping ratio of coral sand, Pando et al.[6] conducted undrained cyclic triaxial tests and resonant column tests on Spanish Cabo Rojo coral sand and quartz sand, and found that the dynamic shear modulus and damping ratio of coral sand were lower than those of the quartz sand. Pham et al.[7] studied the influence of the particle size distribution on the maximum shear modulus through bender element tests. The results show that the effective confining pressure p_0', and relative density D_r, have important effects on G_{max} of coral sand, and the G_{max} of coral sand is higher than that of quartz sand under the same conditions, and the particle gradation, shape and angularity all have important influences on G_{max} of coral sand. Carraro et al. [8] investigated the dynamic shear modulus and damping ratio of coral sand from the west-north sea of Australia using resonant column tests, and found that dynamic shear modulus and damping ratio of coral sand were larger than those of quartz, and the decay rate of G of coral sand with increasing strain was faster compared to quartz sand. These studies show that there are considerable differences for the dynamic shear modulus and damping ratio of coral sands in different areas.

Few research has been conducted on the dynamic characteristics of coral sands in China. Li Jianguo[9] analyzed the effect of initial principal stress direction on liquefaction characteristics and dynamic strength of saturated coral sand using vertical-torsional shear tests. Yu Haizhen[10] investigated the liquefaction mechanism and dynamic strength characteristics under complex initial stress state and dynamic stress conditions. However, these studies were relatively simple

Received: 19 December 2018 Received: 28 April 2019
This work was supported by the National Natural Science Foundation of China (51678299), the National Key R&D Program of China (2017YFC1500403) and the Postgraduate Research and Practice Innovation Program of Jiangsu Province (KYCX18_1057).
First author: LIANG Ke, male, born in 1991, PhD candidate, Research interest: dynamic properties of coral sand. E-mail: liangk91@163.com
Corresponding author: CHEN Guo-xing, male, born in 1963, PhD, Professor, Research interest: soil dynamics and geotechnical earthquake engineering, E-mail: gxc6307@163.com

in terms of dynamic shear modulus and damping ratio. Ma Weijia et al.[11] further studied the liquefaction characteristics of saturated coral sands. Due to the increasing number and scale of coral reef construction in Nansha Islands, it is necessary to perform experiments to further study the G and λ of saturated coral sand in Nansha Islands.

Currently, there are comprehensive knowledge on the dynamic shear modulus and damping ratio of terrigenous sandy soil and gravel. G and λ are mainly influenced by confining pressure and relative density[12-13], as well as other factors, such as the particle gradation, particle size, consolidation and load conditions, etc[14-17]. In this paper, strain-controlled undrained multistage cyclic triaxial tests were carried out on coral sand from Nansha Islands to investigate the influences of effective confining stress p_0' and relative density D_r on G and λ at different shear strain amplitudes γ_a.

2 Physical properties of coral sand

The physical and mechanical properties of coral sand are considerably different from terrigenous sediments. The coral sand used in the tests was white, and was acquired from an island in Nansha. The main minerals of this coral sand are aragonites, calcites and magnesium-rich calcites, with mass percentages of 55.5%, 41.5%, and 3.0%, respectively. Fig.1 is the scanning electron microscope image and shows that the coral sand particles are highly angular, irregular in shape, slender and flaky particles with many inner pores.

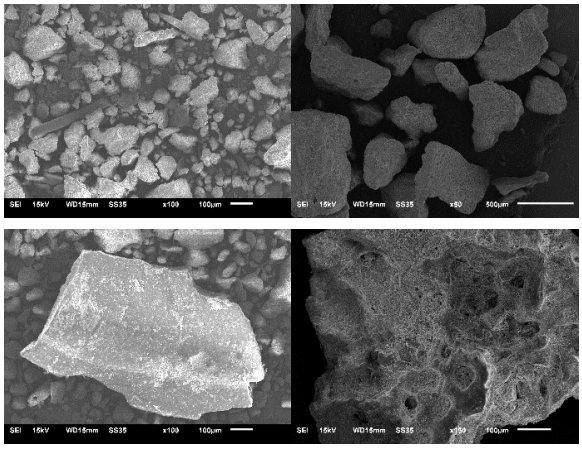

Fig.1 Scanning electron microscope images of coral sand particles

The original sample has a wide range particle size distribution, with a few particles having size greater than 100 mm. The gradation curve of coral sand after removing the particles with size greater than 50 mm is shown in Fig.2.The particles with size greater than 2 mm take up a small percentage of 15.4%. According to the geologic investigation data reported by Shan Huagang et al.[18], the coral sand within a depth of 10 m is mainly medium sand and fine sand, with some gravels in certain areas. Based on the theory of particle contact, the coarse particles when suspending among finer particles have almost no effect on the mechanical properties of soil[19]. In order to satisfy the requirement for triaxial tests that the maximum particle size should be smaller than 1/6 of the specimen diameter[20], the similar gradation method, equivalent mass replacement method, removing method, and mixing method are typically used to eliminate the scale effect of coarse particles. According to previous study[21], the coral gravels with size greater than 2 mm were removed in this study, and the grain size distribution is shown in Fig.2. Due to the fragile behavior of coral sand, the minimum void ratio e_{min} was measured by shaking under static compression in a container. The physical properties of coral sand are summarized in Table 1. According to the "*Engineering Classification Standard of Soil" of China* (GB/T 50145-2007)[22], this coral sand is classified as poorly graded sand (SP).

3 Strain-controlled undrained multistage cyclic triaxial tests

3.1 Test equipment

A series tests were conducted using a hydraulic-servo cyclic triaxial test equipment from GCTS. This equipment can apply dynamic loading in five modes independently, including axial loading, torsional loading, external confining pressure, internal confining pressure, and back pressure. It can be used to conduct dynamic testing on solid specimen or hollow specimen with confining pressure smaller than 3 MPa. In the tests, the range of axial displacement sensor is ±7.5 mm, and the range of internal axial load sensor is ±4 kN, both of which have accuracy higher than 0.1%FS (FS is the full scale). Fig.3 shows the testing system, including five components.

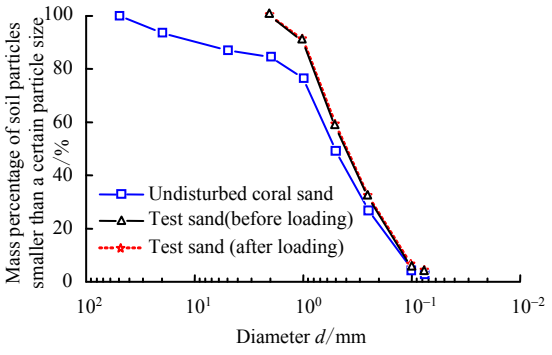

Fig.2 Grain size distribution curves of coral sand

Table 1 Physical properties of coral sand

Specific gravity G_s	Maximum void ratio e_{max}	Minimum void ratio e_{min}	Mean grain size d_{50}/mm	Coefficient of uniformity C_u
2.77	1.14	0.69	0.40	4.47

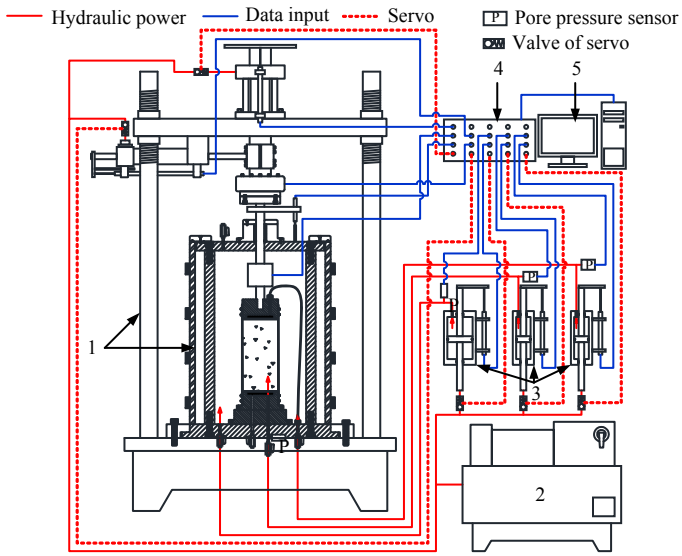

1—Cyclic triaxial equipment and axial, torsional loading apparatus; 2—Oil pump system; 3—Hydraulic controller providing inner, external confining pressure and back pressure; 4—SCON-2000 data collection and digital control system; 5—Computer and GCTS software operating system

Fig.3 Schematic diagram of GCTS triaxial apparatus

3.2 Specimen preparation and saturation

The primary goal of these tests is to study the dynamic shear modulus and damping ratio of saturated coral sand under isotropic consolidation. The specimen was 50 mm in diameter and 100 mm in height, and were prepared using static compression method to avoid particle crashing of coral sand. The coral sand was equally divided into five pieces according to mass calculated based on relative density and volume, and then was placed into the mold and compressed under static loading to the target height of each layer . For dense specimen, in addition to static loading, the mold was knocked using rubber hammer for ease of compression, which would not cause particle crashing. The specimen was then placed into the triaxial cell, and a negative pressure of 15 kPa was applied inside the specimen. The relative density of specimen was calculated using the measured average diameter (excluding the thickness of rubber membrane) and height of the specimen after installing. After test setup, vacuum was applied to the specimen for saturation according to ASTM D3999-11[20], and the back pressure was increased to 400 kPa. The specimen was considered as saturated, when the B value was greater than 0.95[20].

3.3 Test scheme

Isotropic consolidation was applied at least 6h after saturation, and the volume change of specimen was measured after consolidation and the corresponding D_r was calculated. Strain-controlled undrained multistage cyclic triaxial tests were then conducted, with axial strain ε_a increasing from 1×10^{-5} to 1×10^{-2}. At the end of each of loading stage, recovering was allowed at least 15 min for the specimen to return to the initial consolidation condition, and then the next loading stage was applied. Each loading stage contains five cycles at the frequency of 0.5 Hz. D_r ranged between 31% and 76%, and p_0' has four different values of 50, 100, 200 and 300 kPa. The details of these tests are shown in Table 2.

4 Results and analyses

Deviator σ and axial strain ε can be measured directly from cyclic triaxial tests. For the saturated specimen, no volume change was allowed under undrained condition, and thus the Poisson's ratio of the specimen can be assumed to be 0.5. According to the theory of elasticity, the shear stress $\tau=\sigma/2$ during loading and the shear strain $\gamma=1.5\varepsilon$[13, 23].

Under cyclic loading, dynamic shear modulus is defined as the slope of the line connecting the two ends of the stress-strain hysteresis loop, thus $G=\tau_a/\gamma_a$, and the damping ratio is associated with the area of the hysteresis loop[13]. In this paper, the dynamic shear modulus and damping ratio were calculated using the method proposed by Liang et al.[24] based on autocorrelation functions. The average stress amplitude τ_a and the average strain amplitude γ_a during five cycles were calcuated based on the stress and strain time histories using the autocorrelation functions. Then, the average dynamic shear modulus G corresponding to γ_a in the five cycles were calculated. Finally, the cross-correlation functions of the stress and strain time histories were used to calculate the phase difference between these two time histories, and then the average damping ratio λ of five cycles was calculated. This method can eliminate the effect of testing noise and improve the accuracy of G and λ calculation from cyclic traixial test results, and improve an order of magnitude smaller for the range of G and λ measurement using cyclic triaxial tests for the same condition. In this paper, the tests conducted using the GCTS cyclic triaxial test equipment could accurately measure G and λ in the strain range of 10^{-5}−10^{-2}.

Table 2 Specimen data and test results

Number	Specimen number	Initial condition		Test result			
		p_0' /kPa	D_r/%	G_{max}/MPa	γ_0 /%	λ_{min} /%	λ_{max} /%
1	50-1	50	31.0	36.82	0.059	1.84	19.90
2	50-2	50	52.8	42.91	0.063	2.49	18.47
3	50-3	50	64.1	43.62	0.067	1.98	17.08
4	50-4	50	73.7	49.33	0.066	1.68	16.27
5	100-1	100	35.4	58.33	0.072	2.03	20.06
6	100-2	100	43.3	60.33	0.074	2.22	18.27
7	100-3	100	47.3	61.43	0.079	2.25	19.41
8	100-4	100	52.0	63.64	0.082	1.08	17.19
9	100-5	100	55.2	69.37	0.076	2.41	18.20
10	100-6	100	56.7	70.61	0.083	1.88	17.48
11	100-7	100	63.0	69.72	0.075	1.60	16.87
12	100-8	100	67.0	72.20	0.080	2.22	17.20
13	100-9	100	71.5	75.55	0.080	2.24	17.65
14	100-10	100	72.0	78.92	0.073	2.67	16.98
15	100-11	100	75.2	79.57	0.074	2.28	16.80
16	200-1	200	38.7	92.46	0.102	1.06	19.00
17	200-2	200	55.5	101.32	0.099	1.07	17.34
18	200-3	200	60.0	109.08	0.093	1.65	17.74
19	200-4	200	70.0	109.79	0.103	1.07	16.56
20	200-5	200	75.5	118.54	0.096	1.05	16.63
21	300-1	300	47.1	125.64	0.108	1.02	18.83
22	300-2	300	59.5	133.92	0.112	1.66	17.27
23	300-3	300	67.8	149.75	0.110	1.02	16.97
24	300-4	300	68.7	147.30	0.114	2.00	17.30
25	300-5	300	76.0	155.84	0.106	2.07	16.62

Note: λ_{min} and λ_{max} are the maximum and minimum damping ratio, respectively.

4.1 Maximum dynamic shear modulus

The maximum dynamic shear modulus of soil G_{max} is typically chosen as the dynamic shear modulus at $\gamma_a=1\times10^{-6}$. However, it is too difficult to measure the dynamic properties at such small strain levels using cyclic triaxial tests, and thus G_{max}[13] has to be determined through extrapolation. The cyclic shear stress-strain backbone curve can be described using the HD hyperbolic model[25]. In this model, $1/G = a + b\gamma_a$, and then $1/G - \gamma_a$ can be fit using test data. The intercept is a, and thus $G_{max}=1/a$. The results for G_{max} of coral sand are shown in Table 2.

Previous studies indicated that the maximum dynamic shear modulus is mainly influenced by soil type, void ratio, and mean effective confining pressure. The results for G_{max} of coral sand under different conditions are shown in Fig.4. Using Hardin model, G_{max} of coral sand can be expressed as:

$$G_{max}=402.95\times\frac{(2.659-e)^2}{1+e}\times p_a\times\left(\frac{p_0'}{p_a}\right)^{0.625} \quad (1)$$

where p_a is the atmospheric pressure (100 kPa).

Fig.5 shows the comparison of G_{max} for coral sand from experiments and calculated values using different empirical formulas. Saxena et al.[26] proposed a relationship for G_{max} with e and p_0' for Monterey 0# standard silica sand (SP):

$$G_{max}=\frac{428.2}{0.3+0.7e^2}p_a\left(\frac{p_0'}{p_a}\right)^{0.574} \quad (2)$$

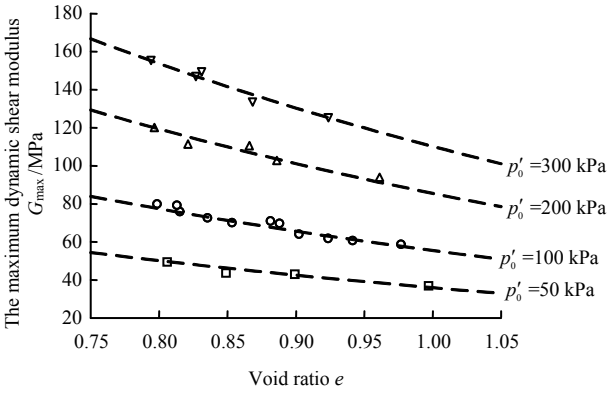

Fig.4 G_{max} of coral sand

Menq[16] proposed a more sophisticate relationship on G_{max}, which accounts for the influences of coefficient of uniformity C_u and mean grain size d_{50}:

$$G_{max}=\left(671C_u^{-0.2}\right)e^{\left[-1-(d_{50}/20)^{0.75}\right]}p_a\left(\frac{p_0'}{p_a}\right)^{0.48C_u^{0.09}} \quad (3)$$

As shown in Fig.5, the values of G_{max} predicted using the two methods for terrigenous sandy soil are similar, but the predicted values are approximately 30% smaller than the measured value of coral sand, which indicates that the G_{max} of coral sands is larger than terrigenous sandy soil.

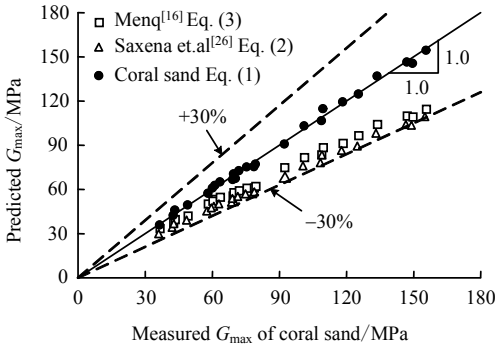

Fig.5 Comparison between the predicted G_{max} and measured G_{max} of coral sand

4.2 Dynamic shear modulus reduction curve

The ratio of dynamic shear modulus G/G_{max} is typically used to describe the relationship of dynamic shear modulus with increasing strain. Fig.6(a) shows that the G/G_{max}– γ_a curves are different for different p_0', and the curve moves up with increasing p_0', which indicates that the nonlinearity of coral sand becomes weaker. But D_r has almost no influence on the curves under the same p_0', as shown in Fig.6(b).

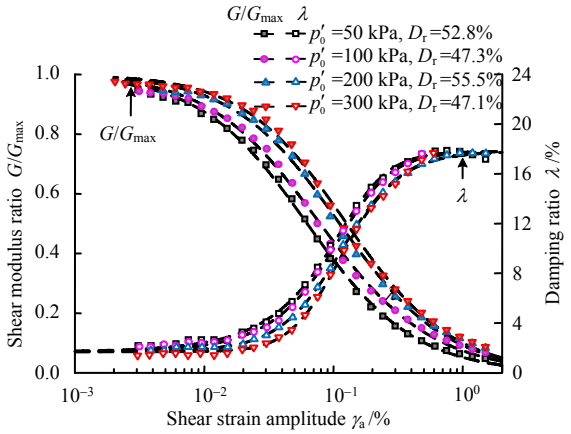

(a) D_r=47.1%–55.5%

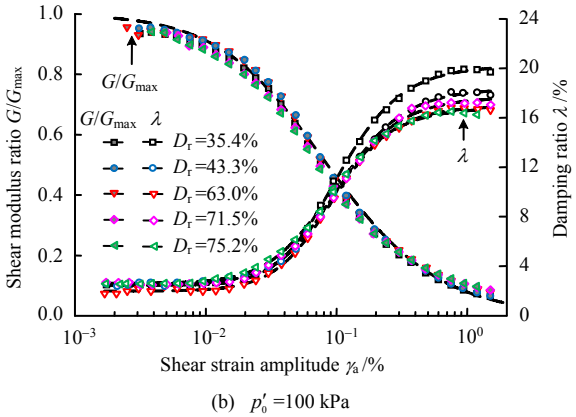

(b) p_0' =100 kPa

Fig.6 Curves of shear modulus ratio and damping ratio for coral sand

4.2.1 Normalized dynamic shear modulus

Davidenkov model[27] is used to predicted the relationship of G/G_{max} and γ_a, as expressed:

$$\frac{G}{G_{max}} = 1 - \left[\frac{(\gamma_a/\gamma_0)^{2\beta}}{1+(\gamma_a/\gamma_0)^{2\beta}} \right]^{\alpha} \tag{4}$$

where α and β are fitting parameters. This model is widely used. For simplicity, the value of reference shear strain γ_0 is chosen as the value of γ_a [13, 16] corresponding to G/G_{max} =0.5, and the results of γ_0 for each specimen are shown in Table 2.

Fig.7 shows the normalized dynamic shear modulus reduction curves with γ_a/γ_0 as the variable for coral sand. It can be seen that the discreteness of data about G/G_{max} is small, which indicates that the method can effectively eliminate the influence of p_0' on the shape of G/G_{max} curve. The best fitting parameters are α = 1.03 and β = 0.52.

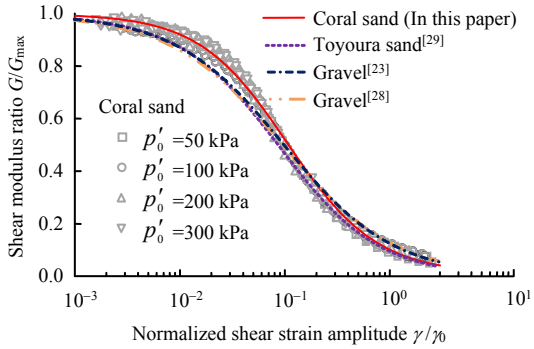

Fig.7 Relationships between shear modulus ratios and normalized shear strain of sandy soils and gravels

Based on the results from previous studies[23,28-29], the dynamic shear modulus reduction curves of different types of terrigenous sandy soils are processed using the method above and are plotted as G/G_{max} - γ_a/γ_0 curves as shown in Fig.7. It can be seen that: (a) the curves for different types of terrigenous sandy soils and gravels are almost the same; (b) when γ_a/γ_0 < 1.0, the decay rate of the curve for coral sand is obviously smaller than for terrigenous sandy soil and gravel; (c) when γ_a/γ_0 > 1.0, the differences of curves for coral sand and terrigenous sandy soil and gravel are relatively small.

4.2.2 Reference shear strain

The relationship of reference shear strain γ_0 and p_0' for coral sand is plotted in Fig.8(a). Results indicates that D_r has relatively small influence on γ_0, while p_0' has larger influence, and γ_0 increases with increasing p_0'. The relationship can be expressed as follows:

$$\gamma_0 = 7.8\times10^{-4}\times(p_0'/p_a)^{0.319} \tag{5}$$

Fig.8(b) compares the γ_0 - p_0' curves for coral sand and terrigenous sandy soil and gravel. Under the same confining pressure, γ_0 for coral sand and terrigenous sandy soil are larger than for terrigenous gravel. The slope of the lg γ_0-lg p_0' curve for coral sand is similar with terrigenous gravel but smaller than terrigenous sandy soil. The main reason is that the coral sand has rough surface and high angularity, and its shape is similar to gravel[28], which produces stronger restriction among the particles and thus leads to weaker influence of confining pressure on γ_0. Hence, the slopes of the lg γ_0-lg p_0' curves for coral sand and terrigenous gravel are smaller than

terrigenous sandy soil.

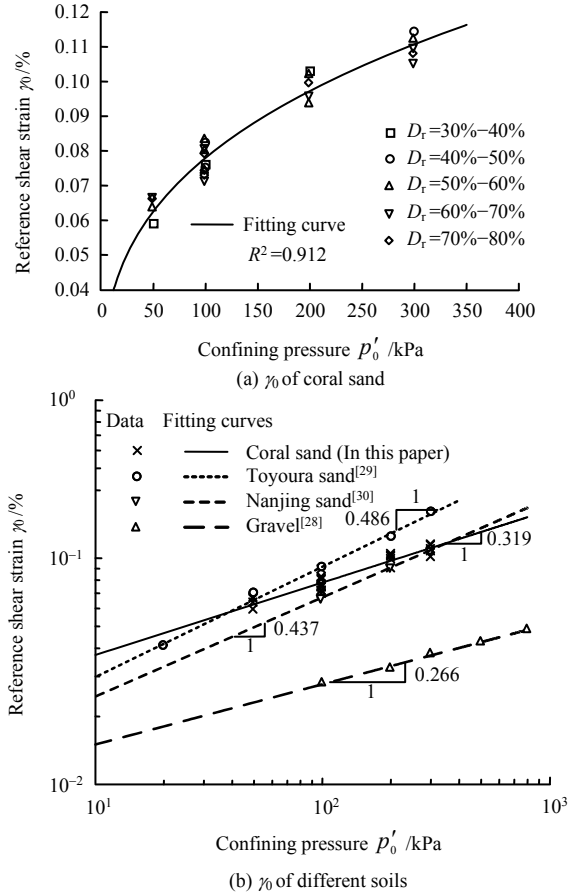

Fig.8 Relationships between reference shear strain and confining stress of sandy soils and gravels

4.2.3 Boundaries of normalized dynamic shear modulus

The coefficient of determination, derived from the regression analysis between the predicted values from the model in this paper and experimental values, R^2 = 0.996. This indicates that the predication model has good accuracy. Fig.9 shows the curves for mean value of G/G_{max} under different confining pressures, and the upper boundary and the lower boundary[12,23,29] of the modulus reduction curves for different types of sand and gravel under similar confining pressures. In this figure, the reduction curves for coral sand and terrigenous sandy soil and gravel are different: (a) under similar confining pressures, the difference between the upper and the lower boundaries of the coral sand curve is smaller than for terrigenous sand and gravel; (b) the decay rate of G/G_{max} with γ_a for coral sand is smaller than for terrigenous sand and gravel, and the upper boundary of coral sand is higher than terrigenous sand and gravel, especially for 0.004%< γ_a < 0.060%. Results indicate that current empirical formulas for predicting G/G_{max} for terrigenous sand and gravel are not applicable for coral sand.

4.3 Damping ratio curve

Typical results of damping ratio for coral sand are shown in Fig.6 and indicates that the influences of p_0' and D_r on λ of coral sand are different at different strain amplitudes. (a) when $\gamma_a < 1\times10^{-4}$ or $\gamma_a > 5\times10^{-3}$, the influence of p_0' on λ is small; when $1\times10^{-4} < \gamma_a < 5\times10^{-3}$, λ decreases with increasing p_0', but the influence of p_0' on λ becomes weaker with increasing γ_a. (b) when $\gamma_a < 1\times10^{-3}$, the influence of D_r on λ is small λ; when $\gamma_a > 1\times10^{-3}$, λ decreases with increasing D_r, and the influence becomes stronger with increasing γ_a; when γ_a gets close to or exceeds 1%, the curves of λ gradually become flat. The main reason is that when γ_a is relative large, the effective confining pressure decreases significantly due to rapid increase of pore pressure, and thus the initial effective confining pressure does not have a major influence on λ. Particle contacts depend on the relative density. The larger D_r is, the stronger particle contacts are. As a result, λ of coral sand decreases with increasing D_r.

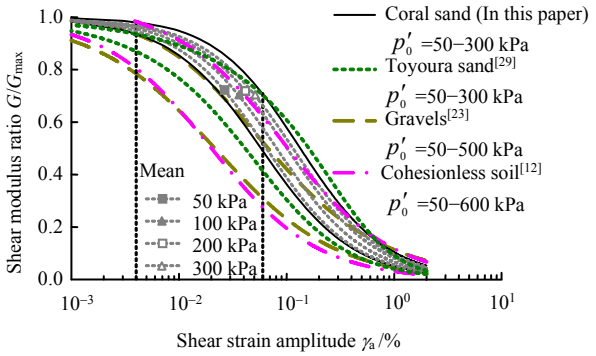

Fig.9 Shear modulus reduction curves of different sandy soils and gravels

Harding et.al[25] found that the dynamic shear modulus G/G_{max} are correlated with damping ratio λ:

$$\lambda = f\left(G/G_{max}\right) \tag{6}$$

In this paper, λ are normalized as follows:

$$\lambda_{nor} = \left(\lambda - \lambda_{min}\right)/\left(\lambda_{max} - \lambda_{min}\right) \tag{7}$$

where λ_{nor} is the normalized damping ratio.

Theoretically, for perfect viscous plastic material, λ_{min} = 0, but Chen et.al[13,17] found that there is energy dissipation even at very small strain amplitude based on triaxial test results of Nanjing fine sand and gravel, which are consistent with findings from Rollins et al.[23] and Kokusho[29]. Chen et al.[13, 17] assumed that λ_{min} could be chosen as the damping ratio at $\gamma_a = 10^{-5}$, because when shear strain is at the order of magnitude 10^{-5}, λ of coral sand is relatively small and increases very slowly, and λ becomes stable when γ_a reaches to 5×10^{-3}. For specimen under different conditions, λ_{min} and λ_{max} could be chosen as the damping ratio at $\gamma_a = 5\times10^{-5}$ and 7×10^{-3}, respectively. The results are shown in Table 2.

The relationship between λ_{nor} and G/G_{max} is shown in Fig.10. It can be seen that all data points are located in a narrow belt, and the correlation between λ_{nor} and G/G_{max} are good. The equation for the best fit curve is:

$$\lambda_{nor} = 0.77\times\arctan\left[\left(\frac{G}{G_{max}} + 0.54\right)^{-4.46}\right] - 0.12 \tag{8}$$

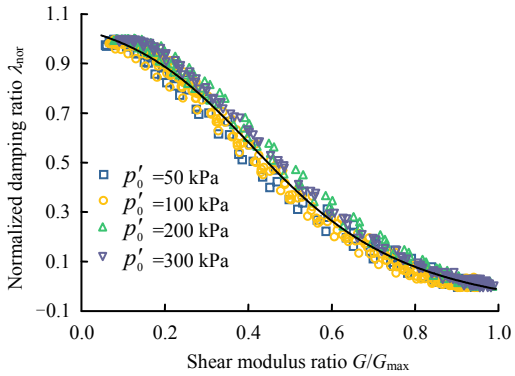

Fig.10 Relationships between normalized damping ratios and shear modulus ratios

The damping ratio of coral sand is expressed as:

$$\lambda = \lambda_{min} + (\lambda_{max} - \lambda_{min})\lambda_{nor} \quad (9)$$

λ_{min} is chosen as the mean value of minimum damping ratio, 1.8%, because the effects of p_0' and D_r on λ_{min} is relative small. Fig.11 indicates that λ_{max} is mainly affected by D_r and decreases with increasing D_r. These two parameters have an approximately linear relationship expressed as:

$$\lambda_{max} = 21.98\% - 7.27\% \cdot D_r \quad (10)$$

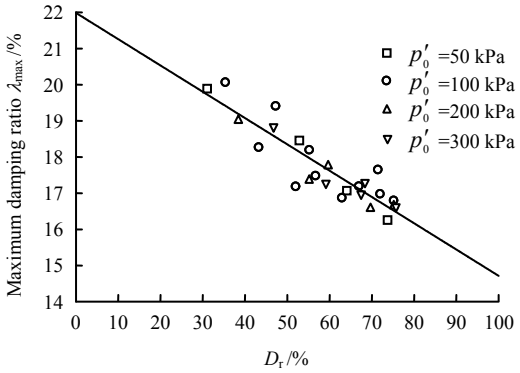

Fig.11 Relationships between maximum damping ratios and relative densities

According to the empirical formulas for λ of coral sand, Eq. (8) to (10), and G/G_{max}, Eq. (4) and (5), Fig.12 shows the damping ratio for different conditions, including D_r =45% under p_0' = 50 kPa, 100 kPa and 200 kPa, and p_0' =100 kPa with D_r= 30%, 45%, 60% and 75%. Results indicate that the damping ratio prediction model can capture the effects of p_0' and D_r on λ for different strain amplitudes. The coefficient of determination, derived from the linear regression analysis between the predicted and measured values, is 0.992, indicating good prediction accuracy.

Fig.13 shows comparison of the damping ratio curves for coral sand and terrigenous sandy soil and gravel[23, 29]. It can be seen that λ of coral sand is smaller than Toyoura sand, and the difference of coral sand between the upper and the lower boundaries is smaller than the terrigenous sandy soils. There are some distinct differences between the λ curves for these two types of soils: (a) when γ_a < 0.02% and γ_a >0.30%, λ of coral sand increases with increasing γ_a, and the increasing rate is significantly smaller than that of the terrigenous sandy soil. Especially a the order of magnitude of γ_a is 10^{-5}, the λ of coral sand is nearly constant. (b) when the order of magnitude of γ_a is 10^{-4}, the lower boundary of the λ curve of coral sand is lower than that of the terrigenous sandy soils. Therefore, the empirical formulas for terrigenous sandy soil are not applicable for coral sand.

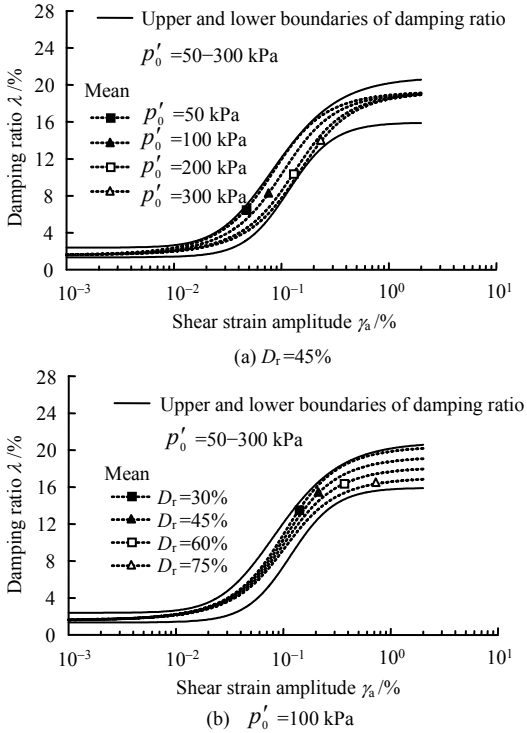

Fig.12 Predicted damping ratios of coral sand

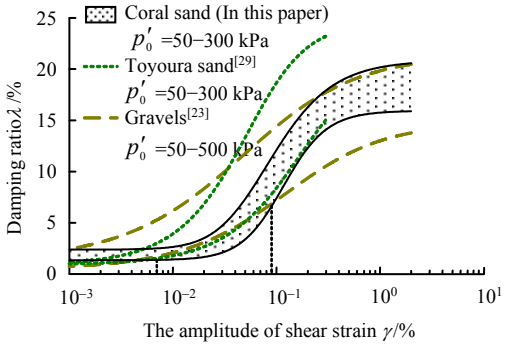

Fig.13 Damping ratios curves of different soils

4.4 Effects of increasing pore pressure, reconsolidation and particle crashing

During multistage loading, reconsolidation was allowed after each loading stage for recovering of the initial consolidation state. Drainage occurred during the reconsolidation process, when the strain amplitude exceeded a certain value, resulting in decrease in volume and increase in D_r. On the other hand, the specimen was loaded for five cycles under undrained condition, during which residual pore pressure u accumulated, when the strain amplitude exceeded a certain value. G of soil mass increased with increasing D_r and decreased with increasing u. The influences of the above two factors would be nearly counteracted when calculating the dynamic shear modulus using the hysteretic loop of certain cycles for each loading stage. According to Eq.(8), the normalized

damping ratio, λ_{nor}, can be correlated with G/G_{max}. Hence, only the influences of D_r and u on G are verified below.

The verification process (undrained cyclic loading test in one stage) is described as follow: (a) After specimen saturation and consolidation, pre-cyclic loading of 3−4 cycles with small strain amplitude is conducted with γ_a smaller than 5×10^{-5} to calculate the G_{max} of the specimen, and the details are the same as multistage cyclic loading. Because the strain amplitude of pre-loading is in the nonlinearly elastic range, pre-loading would not have much effects on the state of specimen and following test[16]. (b) Cyclic loading at the frequency of 0.5 Hz with relative large strain amplitue is applied to the specimen under undrained condition in one stage to determine the dynamic shear modulus of undisturbed specimen in the first cycle under relative large strain. Fourteen verification tests are conducted, and the results are shown in Fig.14. G/G_{max} of undisturbed specimen in the first loading cycle is almost the same with those from multistage cyclic triaxial tests. This indicates that the mean value of G, calculated from 5 cycles in each stage from multistage triaxial tests is almost the same as the dynamic shear modulus of undisturbed specimen in the first loading cycle. In other words, the effects of D_r and u variations during multistage cyclic loading tests on G are nearly counteracted.

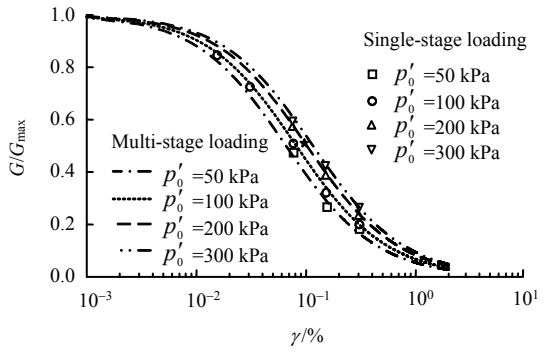

Fig.14 Comparation between G/G_{max} of coral sand obtained from multi- and single-stage cyclic triaxial tests

Particle crashing is one of the most distinct characteristics of coral sand as compared with terrigenous sandy soil, and it has strong effects on the mechanical properties. Sun[31] observed visible particle crashing for coral sand after triaxial compression tests with p'_0 >100 kPa, and crashing becomes easier with increasing confining pressure, shear stress, angularity, particle size, inner pore size, and fraction of flaky fragment. The amplitude of axial strain typically reaches over 15% in triaxial compression tests, but the strain amplitude is much smaller than 15% in the multistage cyclic triaxial loading tests. In this paper, the maximum axial strain amplitude is only 1.0%. Even in the liquefaction tests, the amplitude of axial strain for initial liquefaction indication is only 2.5%[11].

For comparison, Fig.2 also shows the grain size distribution curve for the specimen after multistage cyclic triaxial tests under p'_0 = 300 kPa and D_r =76.0%, which is the easiest crashing condition in this study. It can be seen that from the comparison that no visible crashing was observed for coral sand after multistage cyclic loading. Hardin[32] proposed that the relative breaking ratio B_r could be used to describe the extent of particle crashing after loading. B_r is defined as the ratio of the amount of crashing B_t to the potential of crashing B_p. B_t is the area between the grain size distribution curves before and after crashing for particle size greater than 0.075 mm. B_p is the area of on the top of the initial gradation curve for particle size greater than 0.075 mm. The greater the value of B_r, the more serious the particle crashing would occur after loading. Under the easist crashing condition the crashing ratio B_r is only 0.0096, which indicates that there was almost no particle crashing under the effective confining pressure of 300kPa with γ_a increasing to 1.5% in stages. Therefore, there is no need to consider the influence of particle crashing in this study.

5 Conclusions

(1) Under the same condition, the maximum dynamic shear modulus of coral sand from Nansha Islands is larger than that of terrigenous sand. The G_{max} of coral sand predicted by empirical formula for terrigenous sandy soil is underestimated by approximately 30%.

(2) Under the same confining pressure, the G/G_{max}-γ_a curve for coral sand is higher than terrigenous gravels and sands, and the decay rate of G for coral sand is smaller than terrigenous sand. When the effective confining pressures are close, the difference between the upper and lower boundaries of the G/G_{max}-γ_a curve of coral sand is narrower than that of terrigenous gravels and sands. When $0.004\% < \gamma_a < 0.06\%$, the upper boundaries of coral sand is higher than that of terrigenous sand and gravel.

(3) p'_0 has an apparent influence on λ of coral sand when shear strain is at the magnitude of 10^{-4}, while D_r has a stronger influence on λ when shear strain is at the magnitude of 10^{-3}. When $\gamma_a < 0.02\%$ and $\gamma_a > 0.3\%$, λ of coral sand increases with increasing γ_a, but the increasing rate is much smaller than that of terrigenous sand and gravel. When p'_0 are similar, the difference of upper and lower boundaries of the damping ratio curve is narrower as compared with that of terrigenous sand and gravel. When γ_a is at the magnitude of 10^{-4}, the lower boundary of the damping ratio curve for coral sand is lower than for terrigenous sand and gravel.

(4) The nonlinearity of coral sand is weaker than terrigenous sand and gravel, so the empirical formulas of dynamic shear modulus and damping ratio for terrigenous sand and gravel are not applicable for coral sand. Based on saturated poorly graded coral sand from Nansha Islands, this paper provides empirical formulas of G_{max}, G/G_{max} and λ, which provides reference for evaluation of seismic coral sand site response .

(5) During undrained multistage cyclic triaxial tests, with five cycles in each stage, the mean value of G in each stage can counteract the influence of of D_r and u variations on test results. Particle crashing of coral sand was not observed during undrained multistage cyclic triaxial tests.

References

[1] VAHDANI S, PYKE R, SIRIPRUSANEN U. Liquefaction of calcareous sands and lateral spreading experienced in Guam as a result of the 1993 Guam

earthquake[R]. Buffalo: US National Center for Earthquake Engineering Research, 1994: 117-134.

[2] BRANDES H G, NICHOLSON P G, ROBERTSON I N. Liquefaction of Kawaihae harbor and other effects of 2006 Hawaii earthquakes[C]//Proceedings of the 17th International Offshore and Polar Engineering Conference. Mountain View: [s. n.], 2007: 1169-1176.

[3] SANDOVAL E, PANDO M A, OLGUN C G. Liquefaction susceptibility of a calcareous sand from southwest Puerto Rico[C]//Proceedings of the 5th International Conference on Earthquake Geotechnical Engineering. London: [s. n.], 2011.

[4] SANDOVAL E A, PANDO M A. Experimental assessment of the liquefaction resistance of calcareous biogenous sands[J]. Earth Sciences Research Journal, 2012, 16(1): 55-63.

[5] SHARMA S S, ISMAIL M A. Monotonic and cyclic behavior of two calcareous soils of different origins[J]. Journal of Geotechnical and Geoenvironmental Engineering, 2006, 132(12): 1581-1591.

[6] PANDO M A, SANDOVAL E A, CATANO J. Liquefaction susceptibility and dynamic properties of calcareous sands from Cabo Rojo, Puerto Rico[C]//15th World Conference on Earthquake Engineering. Lisbon: [s. n.], 2012.

[7] PHAM H H G, IMPE P V, IMPE W V, et al. Effects of grain size distribution on the initial strain shear modulus of calcareous sand[C]//XVI ECSMGE Geotechnical Engineering for Infrastructure and Development. Edinburgh: ICE Publishing, 2015: 3177-3182.

[8] CARRARO J A H, BORTOLOTTO M S. Stiffness degradation and damping of carbonate and silica sands[C]//Frontiers in Offshore Geotechnics III. London: Taylor & Francis Group, 2015: 1179-1183.

[9] LI Jian-guo. Experimental research on dynamic behavior of saturated calcareous sand under wave loading[D]. Wuhan: Institute of Rock and Soil Mechanics, Chinese Academy of Sciences, 2005.

[10] YU Hai-zheng. Experimental research on dynamic behavior of saturated calcareous sand under complex stress conditions[D]. Wuhan: Huazhong University of Science and Technology, 2006

[11] MA Wei-jia, CHEN Guo-xing, LI Lei, et al. Experimental study on liquefaction characteristics of saturated coral sand in Nansha Islands under cyclic loading[J]. Chinese Journal of Geotechnical Engineering, 2019, 41(5): 981-988.

[12] OZTOPRAK S, BOLTON M D. Stiffness of sands through a laboratory test database[J]. Geotechnique, 2013, 63(1): 54-70.

[13] CHEN G X, ZHOU Z L, SUN T, et al. Shear modulus and damping ratio of sand - gravel mixtures over a wide strain range[J]. Journal of Earthquake Engineering, 2018, 23(8): 1407-1440.

[14] WICHTMANN T, TRIANTAFYLLIDIS T. Influence of the grain-size distribution curve of quartz sand on the small strain shear modulus G_{max}[J]. Journal of Geotechnical and Geoenvironmental Engineering, 2009, 135(10): 1404-1418.

[15] WICHTMANN T, TRIANTAFYLLIDIS T. Effect of uniformity coefficient on G/G_{max} and damping ratio of uniform to well-graded quartz sands[J]. Journal of Geotechnical and Geoenvironmental Engineering, 2013, 139(1): 59-72.

[16] MENQ F. Dynamic properties of sandy and gravelly soils[D]. Austin: University of Texas at Austin, 2003.

[17] CHEN G X, ZHOU Z L, PAN H, et al. The influence of undrained cyclic loading patterns and consolidation states on the deformation features of saturated fine sand over a wide strain range[J]. Engineering Geology, 2016, 204: 77-93.

[18] SHAN Hua-gang, WANG Ren, ZHOU Zeng-hui. Yongshu reef engineering geology of Nansha islands[J]. Marine Geology & Quaternary Geology, 2000, 20(3): 31-36.

[19] THEVANAYAGAM S, MARTIN G R. Liquefaction in silty soils-screening and remediation issue[J]. Soil Dynamics and Earthquake Engineering, 2002, 22(9-12): 1035-1042.

[20] ASTM International. ASTM D 3999−11 Standard test methods for the determination of the modulus and damping properties of soils using the cyclic triaxial apparatus[S]. West Conshohocken: [s. n.], 2011.

[21] FRAGASZY R J, SU J, SIDDIQI F H, et al. Modeling strength of sandy gravel[J]. Journal of Geotechnical Engineering, 1992, 118(6): 920-935.

[22] Ministry of Water Resources of the Reople's Republic of China. GB/T 50145－2007 Standard for engineering classification of soil[S]. Beijing: China Planning Publishing House, 2008.

[23] ROLLINS K M, EVANS M D, DIEHL N B, et al. Shear modulus and damping relationships for gravels[J]. Journal of Geotechnical and Geoenvironmental Engineering, 1998, 124(5): 396－405.

[24] LIANG Ke, CHEN Guo-xing, HE Yang, et al. An innovative method for the calculation of dynamic modulus and damping ratio based on the theory of correlation function[J]. Rock and Soil Mechanics, 2019, 40(4): 1368-1377.

[25] HARDIN B O, DRNEVICH V P. Shear modulus and damping in soils: design equations and curves[J]. Journal of Soil Mechanics and Foundations Division, ASCE, 1972, 98(SM7): 667-692.

[26] SAXENA S K, REDDY K R. Dynamic moduli and damping ratios for Monterey No.0 sand by resonant column tests[J]. Soils and Foundations, 1989, 29(2): 37-51.

[27] MARTIN P P, SEED H B. One-dimensional dynamic ground response analyses[J]. Journal of the Geotechnical Engineering Division, 1982, 108(7): 935-952.

[28] ZOU D G, GONG T, LIU J M, et al. Shear modulus and damping ratio of gravel material[J]. Applied Mechanics and Materials, 2011, 105: 1426-1432.

[29] KOKUSHO T. Cyclic triaxial test of dynamic soil properties for wide strain range[J]. Soils and Foundations, 1980, 20(2): 45-60.

[30] PAN Hua. Experimental research on dynamic behavior of saturated Nanjing fine sand under complex stress conditions[D]. Nanjing: Nanjing Tech. University, 2011.

[31] SUN Zong-xun. Engineering properties of coral sands in Nansha islands[J]. Tropic Oceanology, 2000(2): 1-8.

[32] HARDIN B O. Crushing of soil particles[J]. Journal of Geotechnical Engineering, 1985, 111(10): 1177-1192.